Cell Reports

Supplemental Information

Synapsin III Acts Downstream of Semaphorin 3A/CDK5 Signaling to Regulate Radial Migration and Orientation of Pyramidal Neurons In Vivo

Laura E. Perlini, Joanna Szczurkowska, Bryan A. Ballif, Alessandra Piccini, Silvio Sacchetti, Silvia Giovedì, Fabio Benfenati, and Laura Cancedda

Supplemental Figures:

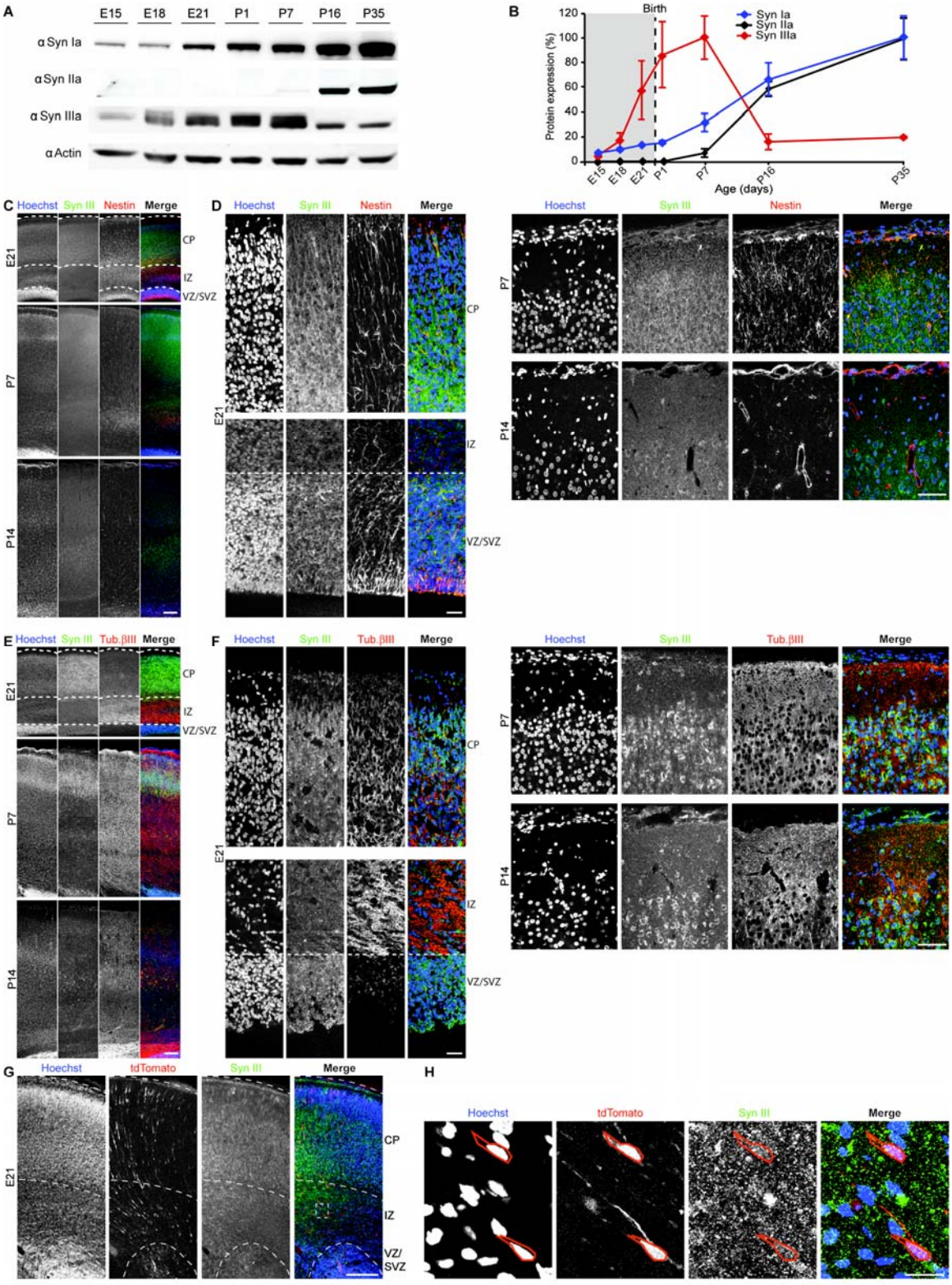

Figure S1 (Related to Figure 1). SynIII expression is temporally and spatially regulated during development. (A) Western blots showing the temporal expression of SynIa, SynIIa and SynIIIa in comparison to actin in lysates of rat brain cortices. **(B)** Quantification of SynIa (blue), SynIIa (black), SynIIIa (red) expression patterns in experiments, as in A. The data were normalized first to actin and then to the maximum detected optical density value for each protein; the values are expressed as means ± SEM (n = 3 animals/age). **(C-F)** Confocal images of SynIII immunoreactivity (green) from coronal sections of the rat somatosensory cortex at various ages. SynIII is abundantly expressed in both the VZ/SVZ and CP at E21, whereas it is concentrated in the CP at P7 and P14. The fluorescence intensity of the images at P7 and P14 was increased for better visualization of SynIII distribution across cortical layers. The slices were counterstained with the nuclear marker Hoechst (blue), and Nestin (C, D, red) or Tubulin βIII (E, F, red). Scale bars: C, E = 200 μm; D, F = 50 μm. **(G)** Confocal images of SynIII immunoreactivity (green) from coronal sections of rat somatosensory cortex at E21 electroporated with tdTomato (red) at E17. Scale bar: 200 μm. **(H)** High-magnification image of cells in the IZ from the cortical slice shown in F, showing the expression of SynIII (green) in migrating cells (red). The slices were counterstained with Hoechst (blue). CP, cortical plate; IZ, intermediate zone; VZ/SVZ, ventricular/subventricular zone. Scale bar: 25 μm.

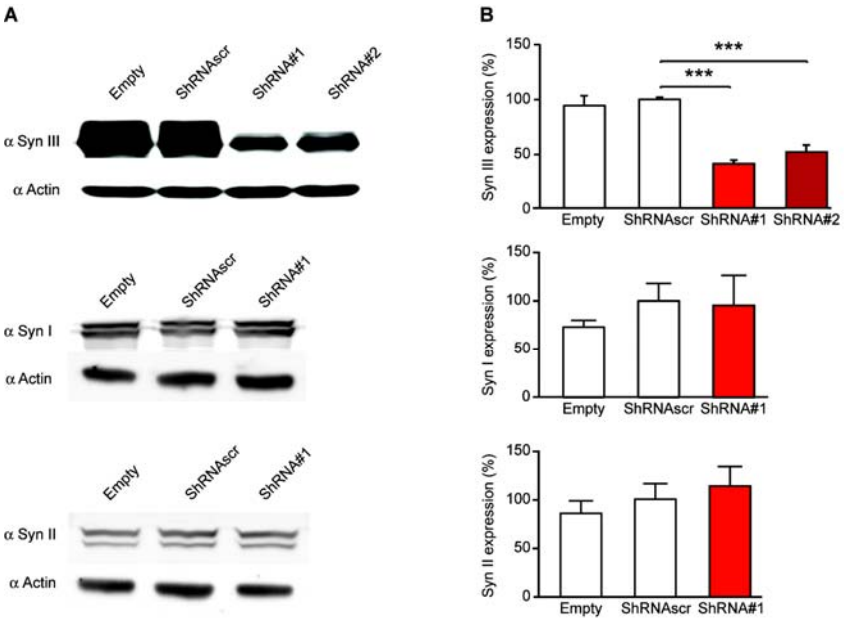
A
Empty
ShRNAscr
ShRNA#1
ShRNA#2
α Syn III
α Actin
α Syn I
α Actin
α Syn II
α Actin
B
Syn III expression (%)
Syn I expression (%)
Syn II expression (%)
***
***
Empty
ShRNAscr
ShRNA#1
ShRNA#2

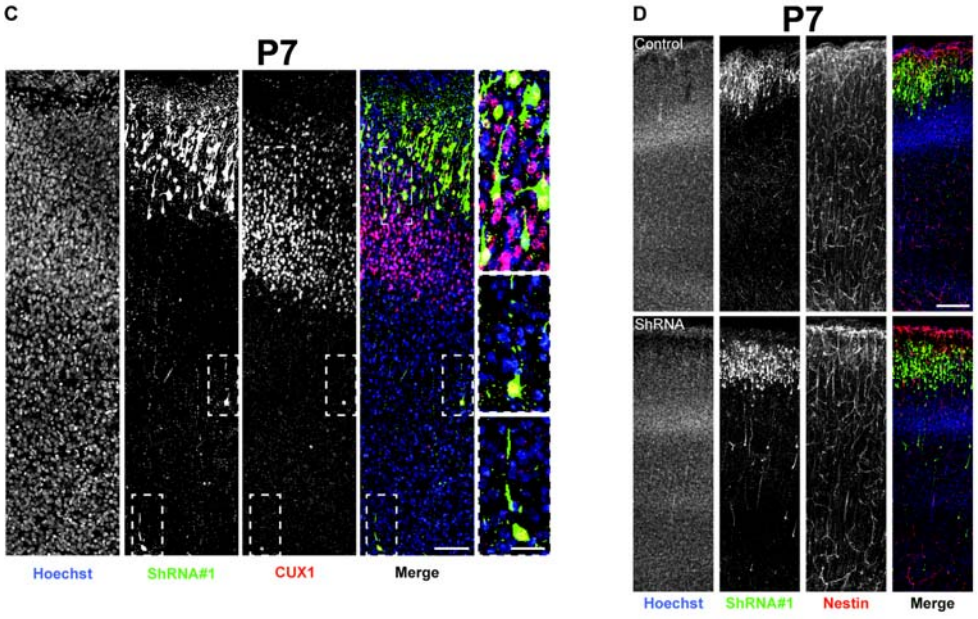
C
P7
Hoechst
ShRNA#1
CUX1
Merge
D
P7
Control
ShRNA
Hoechst
ShRNA#1
Nestin
Merge

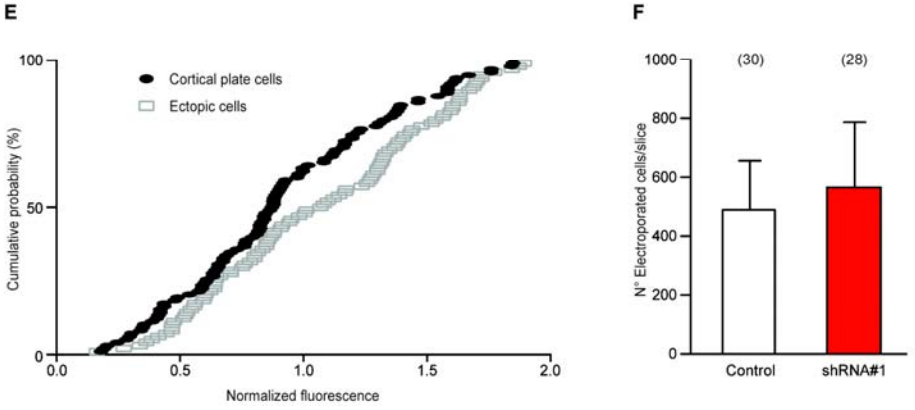
E
Cortical plate cells
Ectopic cells
Cumulative probability (%)
Normalized fluorescence
F
(30)
(28)
N° Electroporated cells/slice
Control
shRNA#1

Figure S2 (Related to Figure 1). ShRNA#1 downregulates SynIII, but not SynI or II, expression, without affecting the RG scaffold, PN fate or proliferation. (A) Representative western blots showing the specificity of ShRNA#1 in downregulating SynIII in comparison to SynI and SynII when exogenously expressed in COS7 cells. **(B)** Quantification of the levels of SynI, II and III, as in A. The data are expressed as mean percentages (± SEM) normalized to the control (ShRNAscr, a scrambled sequence) from n = 3 independent experiments for SynIII and n = 5 independent experiments for SynI and SynII. Asterisks: One-way ANOVA, post-hoc Holm-Sidak vs ShRNAscr, ***p< 0.001. **(C)** Confocal images of CUX1 immunoreactivity (red) from coronal sections of the somatosensory cortex of a rat electroporated at E17 with ShRNA#1 (green) and processed at P7. The slices are counterstained with Hoechst (blue). The fields within the white broken lines are given at high magnification in the right insets. Cell fate was not affected by ShRNA expression. Scale bars: 50 μm and 25 μm (insets). **(D)** Confocal images of nestin immunoreactivity (red) in the somatosensory cortex coronal sections of a rat electroporated at E17 with ShRNAscr (control) or ShRNA#1 (green) and processed at P7. The slices are counterstained with Hoechst (blue). The RG scaffold was not altered by ShRNA expression. Scale bar, 100 μm. **(E)** The cumulative distribution of the average tdTomato fluorescence intensity at the soma of neurons transfected with tdTomato/ShRNA#1 and residing in the CP (black circles) or in ectopic positions (open squares) was quantified as a reporter of SynIII downregulation at P7. The ectopic cells exhibited higher tdTomato fluorescence intensity, consistent with the severe developmental defects that were associated with higher levels of ShRNA expression. Kolmogorov–Smirnov test, *p<0,05. n= 98 cells in total for each group from 3 different brains. **(F)** Histogram showing the total number of counted cells in cortices electroporated with ShRNAscr (control) or ShRNA#1. The data are expressed as mean percentages (± SEM) of the total number of fluorescent cells. No difference is detected between the two groups (Student's *t*-test), indicating that the ShRNA did not affect the proliferation of electroporated cells.

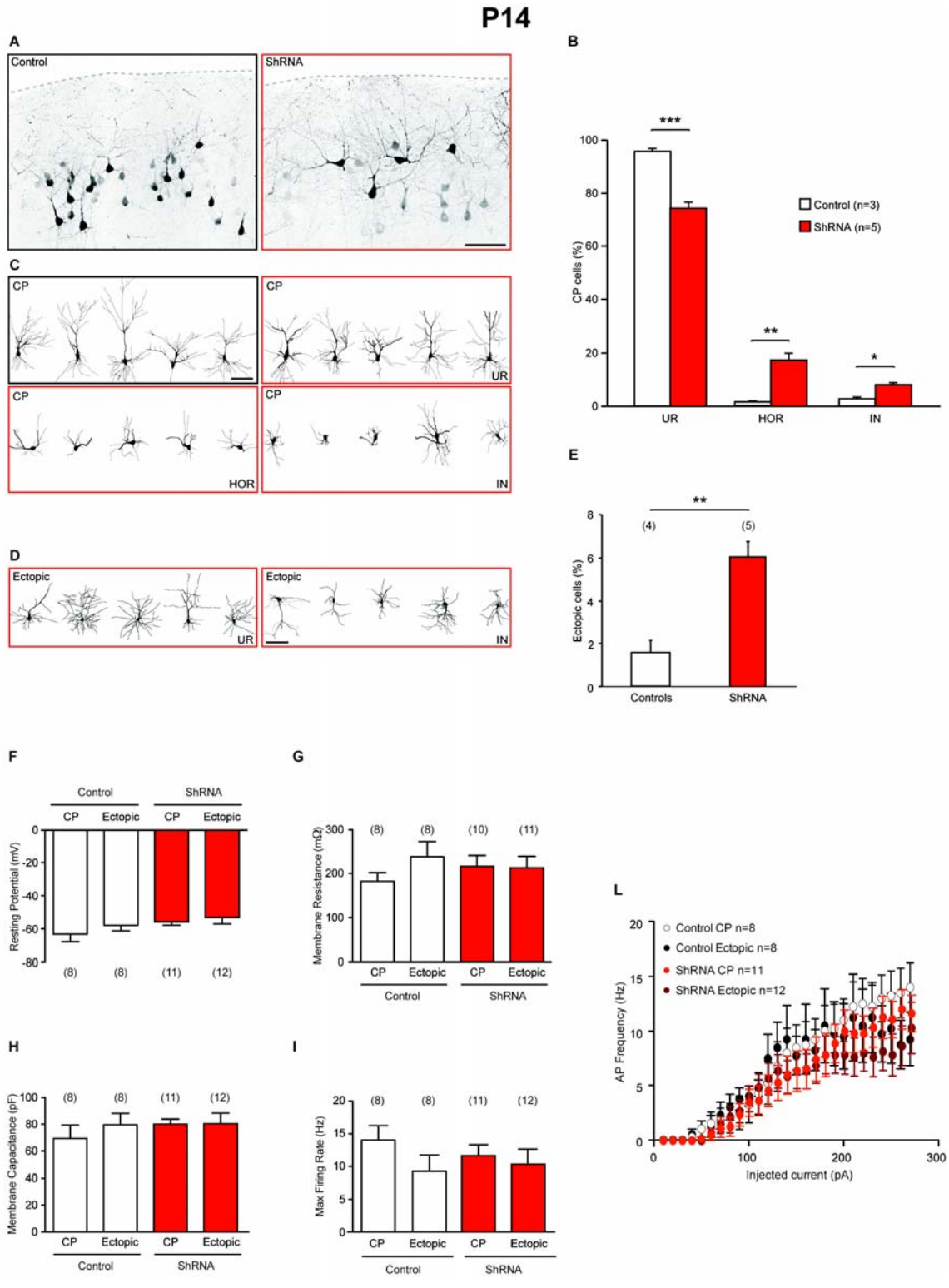
P14
A
Control
ShRNA
B
Control (n=3)
ShRNA (n=5)
CP cells (%)
UR
HOR
IN
C
CP
UR
HOR
IN
D
Ectopic
E
Ectopic cells (%)
Controls
ShRNA
F
Resting Potential (mV)
G
Membrane Resistance (mΩ)
H
Membrane Capacitance (pF)
I
Max Firing Rate (Hz)
L
Control CP n=8
Control Ectopic n=8
ShRNA CP n=11
ShRNA Ectopic n=12
AP Frequency (Hz)
Injected current (pA)

Figure S3 (Related to Figure 1). SynIII downregulation affects neuronal radial migration and orientation, but not the electrophysiological properties of PNs at P14. **(A)** Confocal images of coronal sections of the rat somatosensory cortex at P14 after IUE at E17 with ShRNAscr or functional ShRNA. Scale bar, 50 μm. **(B)** Quantification of the distribution of cells in the three classes defined, as in Figure 1D. The data are expressed as mean percentages (± SEM) of the total number of fluorescent cells at the CP. As observed at P7, misoriented cells were also found in the CP at P14. Asterisks: Student's *t*-test: * $p<0.05$, ** $p<0.01$, *** $p<0.001$. UR = upright, HOR = horizontal, IN = inverted. **(C, D)** Example reconstruction of control and $ShRNA^+$ neurons in the CP (C), as well as $ShRNA^+$ neurons in ectopic positions (D) from images as in A. Scale bars, 50 μm. **(E)** Quantification of the number of control and $ShRNA^+$ neurons that did not complete migration. The data are mean percentages (± SEM) of the total number of fluorescent cells in the section (Student's *t*-test: ** $p<0.01$). The results observed at P14 were similar to those found at P7; some migrating cells resided in deep layers, and misoriented cells were present. **(F-L)** Electrophysiological analysis of transfected neurons at P14. Bar histograms represent the mean (±SEM) of the cell resting potential (F), membrane resistance (G), membrane capacitance (H) and maximal firing rate (I) measured in current-clamp recordings at P12-16 in $ShRNAscr^+$ and $ShRNA^+$ PNs residing in the CP or ectopically. **(L)** Quantification of the action potential frequency with respect to the injected current. The numbers of recorded cells are indicated in parenthesis. The statistical analysis (one-way ANOVA) showed no difference between groups, suggesting that SynIII KD and/or cell position do not affect the basic electrophysiological properties of the treated PNs.

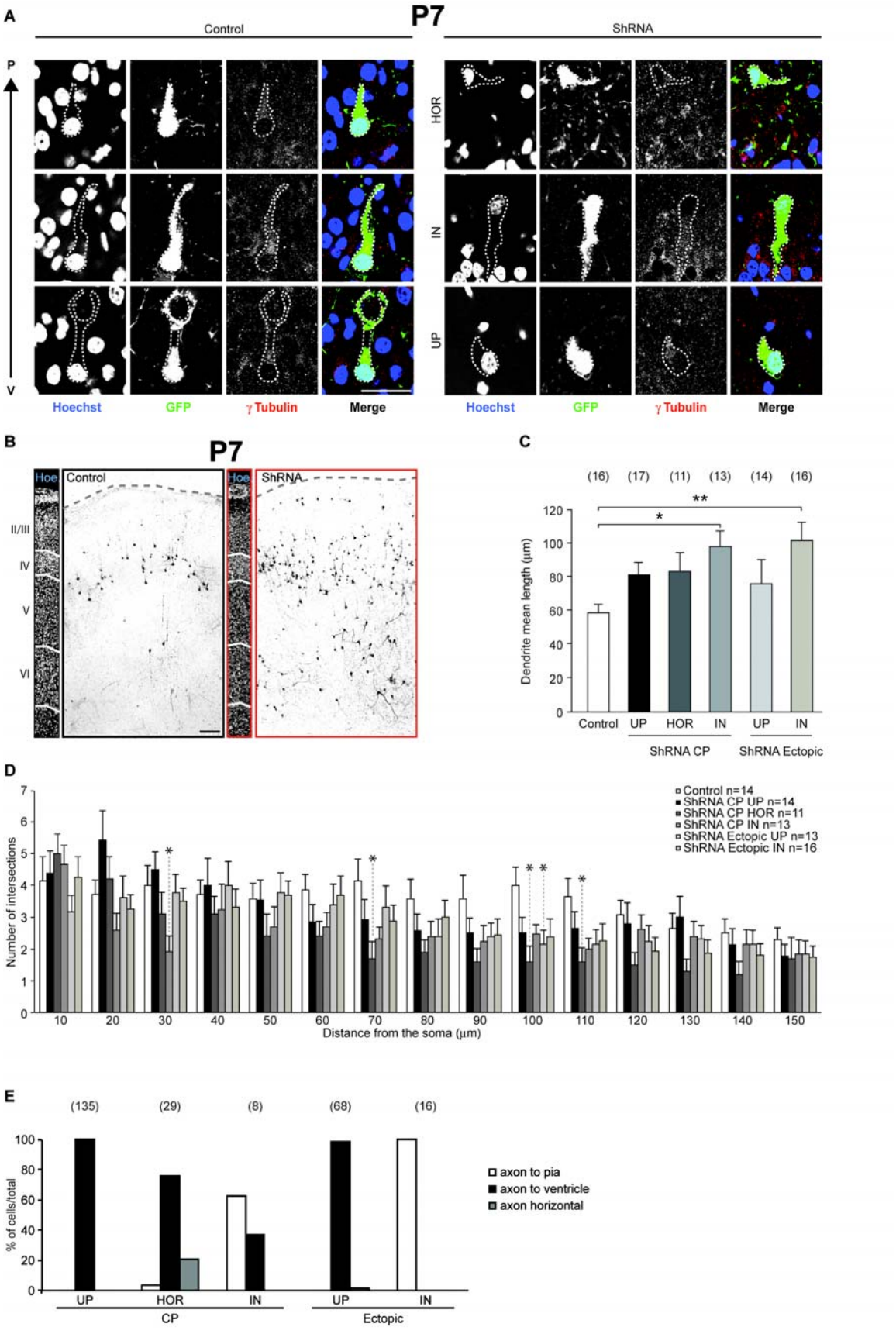
A
P7
Control
ShRNA
P
V
HOR
IN
UP
Hoechst
GFP
γ Tubulin
Merge
B
P7
Hoe
Control
ShRNA
II/III
IV
V
VI
C
(16) (17) (11) (13) (14) (16)
**
*
Dendrite mean length (µm)
Control
UP
HOR
IN
ShRNA CP
ShRNA Ectopic
D
Control n=14
ShRNA CP UP n=14
ShRNA CP HOR n=11
ShRNA CP IN n=13
ShRNA Ectopic UP n=13
ShRNA Ectopic IN n=16
Number of intersections
Distance from the soma (µm)
E
(135) (29) (8) (68) (16)
% of cells/total
axon to pia
axon to ventricle
axon horizontal
CP
Ectopic

Figure S4 (Related to Figure 1). SynIII downregulation affects the morphology and orientation of PNs. (A) Confocal images of γ-tubulin immunoreactivity (red) from coronal sections of the rat somatosensory cortex electroporated at E17 with scramble (control) or ShRNA (green) and processed at P7. The slices are counterstained with Hoechst (blue). γ-tubulin immunoreactivity always colocalized with the apical dendrite, independently of cell orientation. UR = upright, HOR = horizontal, IN = inverted as defined in Figure 1D. P = pia, V = ventricle. **(B)** Confocal images of coronal sections of the rat somatosensory cortex at P7 after IUE at E15.5 with ShRNAscr (control) or ShRNA. The slices are counterstained with Hoechst (blue) to better visualize the cortical layers (numbered on the left). Scale bar, 100 μm. SynIII downregulation also affects deep layer development. **(C, D)** Mean dendrite length (C) and the Sholl analysis (D) of control and $ShRNA^+$ PNs located in the CP or in ectopic positions. The cells are divided into different classes, as defined in Figure 1D. ANOVA on ranks *vs* control, *post-hoc* Dunn's test: *p<0.05, **p<0.01. **(E)** The orientation of axons of $ShRNA^+$ cells located in the CP or in ectopic positions divided into the classes defined in Figure 1D. The number of cells analyzed from 5 brains (3 slices/brain) is shown in parentheses.

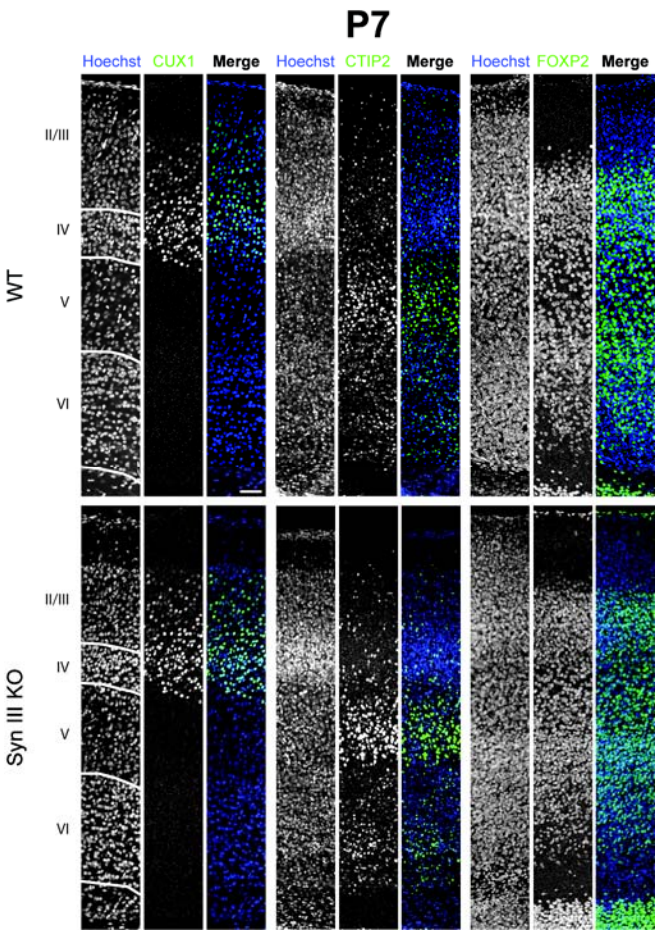

Figure S5 (Related to Figure 3). **SynIII KO mice do not show cortical layering defects.** Confocal images of FOXP2, CUX1 and CTIP2 immunoreactivities (green) in WT and SynIII KO mouse brains at P7. The slices are counterstained with Hoechst (blue). SynIII KO brains did not exhibit any gross defect in cortical layering in comparison to WT brains. Scale bar, 100 μm.

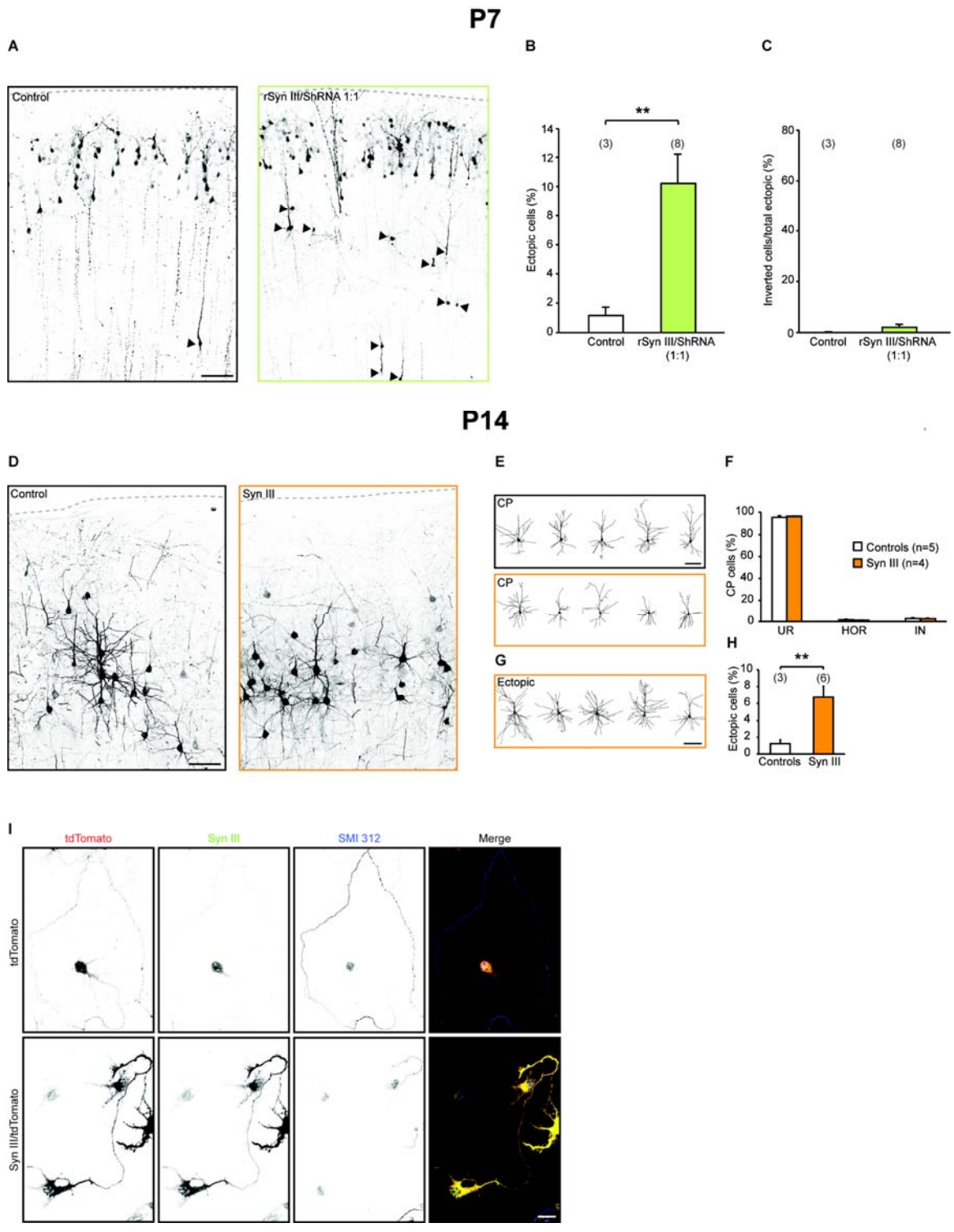
P7
A
Control
rSyn III/ShRNA 1:1
B
**
(3)
(8)
Ectopic cells (%)
Control
rSyn III/ShRNA (1:1)
C
(3)
(8)
Inverted cells/total ectopic (%)
Control
rSyn III/ShRNA (1:1)
P14
D
Control
Syn III
E
CP
CP
G
Ectopic
F
CP cells (%)
Controls (n=5)
Syn III (n=4)
UR
HOR
IN
H
**
(3)
(6)
Ectopic cells (%)
Controls
Syn III
I
tdTomato
Syn III
SMI 312
Merge
tdTomato
Syn III/tdTomato

Figure S6 (Related to Figure 2 and 4). The co-expression of ShRNA and ShRNA-resistant SynIII at a 1:1 ratio rescues the orientation defects of ectopic cells but results in ectopic cell localization. (A) Confocal images of cortical coronal sections from animals at P7 that were transfected with ShRNAscr (control) or rSynIII/ShRNA (1:1 ratio). Scale bar, 100 μm. The arrowheads point to sample PNs that did not complete radial migration. Note that all ectopic cells are in an upright position. **(B)** Quantification of the number of control PNs and rSynIII/ShRNA (1:1 ratio)$^{+}$ PNs that did not complete migration, as in A. The data are mean percentages (± SEM) of the total number of fluorescent cells in the section. ANOVA on ranks, *post-hoc* Dunn's test: **p<0.01. **(C)** Quantification of the number of ectopic PNs that display inverted orientation in control and rSynIII/ShRNA (1:1 ratio)$^{+}$ cortices, as in A. The data are expressed as mean percentages (± SEM) of the total number of ectopic cells in the section. **(D)** Confocal images of cortical coronal sections from animals at P14 transfected with tdTomato only (control) or SynIII/tdTomato. Scale bar, 50 μm. **(E, G)** Reconstruction of representative PNs from control or SynIII-overexpressing cortices; the cells were distributed in the CP (E) or among SynIII-overexpressing ectopic PNs in deep layers (G). Scale bars, 50 μm. **(F)** Quantification of the distribution of cells in the three classes, as defined in Figure 1D. The data are mean percentages (±SEM) of the total number of fluorescent cells at the CP. UR = upright, HOR = horizontal, IN = inverted. **(H)** Quantification of the number of control and SynIII-overexpressing PNs that did not complete migration. The data are expressed as mean percentages (± SEM) of the total number of fluorescent cells in the section. Student's *t*-test, **p<0.01. **(I)** Confocal images of 3 DIV neurons tdTomato^{+} or SynIII^{+} (red). The cells were electroporated by AMAXA with the indicated constructs before plating. The fixed cells were stained for SynIII (green) and SMI 312 (blue). Endogenous SynIII localized to the cell body and the axon, while overexpressed of SynIII displayed a diffuse distribution in all cell compartments. Scale bar, 20 μm.

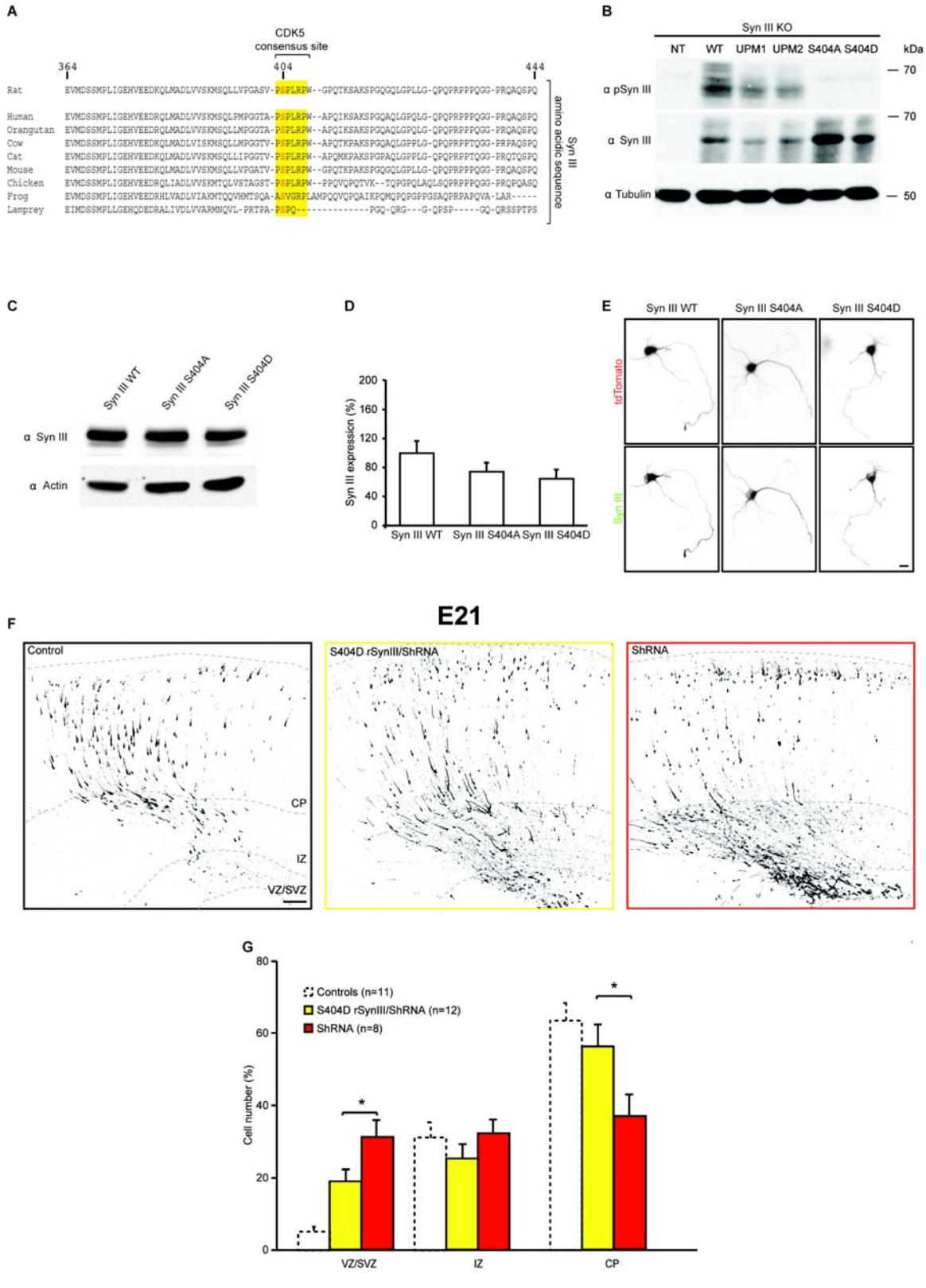
A
CDK5
consensus site
364
404
444
Rat EVMDSSMPLIGEHVEEDKQLMADLVVSKMSQLLVPGASV-PSPLRPW--GPQTKSAKSPGQGQLGPLLG-QPQPRPPPQGG-PRQAQSPQ
Human EVMDSSMPLIGEHVEEDRQLMADLVVSKMSQLPMPGGTA-PSPLRPW--APQIKSAKSPGQAQLGPQLG-QPQPRPPPQGG-PRQAQSPQ
Orangutan EVMDSSMPLIGEHVEEDRQLMADLVVSKMSQLLMPGGTA-PSPLRPW--APQIKSAKSPGQAQLGPQLG-QPQPRPPPQGG-PRQAQSPQ
Cow EVMDSSMPLIGEHVEEDKQLMADLVISKMSQLLMPGGTV-PSPLRPW--APQTKPAKSPGQAQLGPPLG-QPQPRPPTQGG-PRPAQSPQ
Cat EVMDSSMPLIGEHVEEDKQLMADLVVSKMSQLLIPGGTV-PSPLRPW--APQMKPAKSPGPAQLGPPLG-QPQPRPPTQGG-PRQTQSPQ
Mouse EVMDSSMPLIGEHVEEDKQLMADLVVSKMSQLLVPGATV-PSPLRPW--GPQTKPAKSPGQGQLGPLLG-QPQPRPPPQGG-PRQAQSPQ
Chicken EVMDSSMPLIGEHVEEDRQLIADLVVSKMTQLVSTAGST-PSPLRPW--PPQVQPQTVK--TQPGPQLAQLSQPRPPPQGG-PRQPQASQ
Frog EVMDSSMPLIGEHVEEDRHLVADLVIAKMTQQVHMTSQA-ASVGRPLAMPQQVQPQAIKPQMQPQPGPPGSAQPRPAPQVA-LAR-----
Lamprey EIMDSSMPLLGEHQDEDRALIVDLVVARMNQVL-PRTPA-PSPQ--------------PGQ-QRG---G-QPSP-----GQ-QRSSPTPS
amino acidic sequence
Syn III
B
Syn III KO
NT
WT
UPM1
UPM2
S404A
S404D
kDa
α pSyn III
α Syn III
α Tubulin
70
70
50
C
Syn III WT
Syn III S404A
Syn III S404D
α Syn III
α Actin
D
Syn III expression (%)
200
160
120
80
40
0
Syn III WT
Syn III S404A
Syn III S404D
E
Syn III WT
Syn III S404A
Syn III S404D
tdTomato
Syn III
F
E21
Control
S404D rSynIII/ShRNA
ShRNA
CP
IZ
VZ/SVZ
G
Controls (n=11)
S404D rSynIII/ShRNA (n=12)
ShRNA (n=8)
Cell number (%)
80
60
40
20
0
*
*
VZ/SVZ
IZ
CP

Figure S7 (Related to Figure 5,6 and 7). **The pseudo-phosphorylated SynIII mutant is able to significantly rescue the ShRNA-induced migration defect.**

(A) The alignment of the SynIII amino acid sequence across species shows that the consensus sequence for CDK5 (PSPLRP, yellow) is conserved in higher vertebrates. The serine targeted by CDK5 (Ser^{404} in the rat) is highlighted in red. **(B)** Representative western blots showing the specificity of the antibody against SynIII phosphorylated at Ser^{404}. The antibody was probed against SynIII KO neurons (at 3 DIV) that were either non-transfected (NT) or electroporated by AMAXA with WT, S404A and S404D rSynIII or with two unrelated SynIII phosphomutants (UPM1, UPM2). **(C, D)** Representative western blots (C) and quantification of the levels of WT, S404A and S404D rSynIII (D), showing the similar expression of these constructs in COS7 cells. The data are means ± SEM and normalized to the control (ShRNAscr) from n = 8 independent experiments. Statistical analysis (ANOVA on ranks) showed no difference between groups. **(E)** Confocal images of 3 DIV SynIII KO neurons expressing WT, S404A or S404D SynIII. The cells were electroporated by AMAXA before plating. The fixed cells were stained for SynIII (green). WT, S404A and S404D SynIII displayed similar intracellular distributions. Scale bar, 10 μm. **(F)** Confocal images of cortical coronal sections from animals at E21 transfected with ShRNAscr (control), S404D rSynIII/ShRNA or ShRNA. Scale bar, 100 μm. **(G)** Quantification of the number of PNs transfected with ShRNA alone or S404D rSynIII/ShRNA and residing in the VZ/SVZ, IZ, or CP. The data are mean percentages (± SEM) of the total number of fluorescent cells in the section. The distribution of PNs transfected with ShRNA and S404D rSynIII/ShRNA was significantly different in the VZ/SVZ and CP. Student's *t*-test *$p<0.05$). White dashed columns representing controls from Figure 1B are included for comparison.

Supplemental Experimental Procedures:

Generation of Constructs

ShRNAs. ShRNA#1 was designed against the sequence encoding the C domain of SynIII, according to (Elbashir et al., 2001). ShRNA#2 against the SynIII B domain coding sequence was designed with the aid of the BLOCK-iT™ RNAi Express Software (Invitrogen). ShRNA specificity for the mRNA of interest was verified by BLAST aligning with a non-redundant database. The ShRNAs were synthesized by Sigma, annealed *in vitro*, and ligated into pRNAT-U6.3/Hygro vectors (GenScript).

ShRNA sequences:

#1: TAACCAGAATGAAGTCAGGTTttgatatccgAACCTGACTTCATTCTGGTTA

#2: AAGGAGCTAAACAGGCTGGATttgatatccgATCCAGCCTGTTTAGCTCCTT

SynIIIa. pEGFP-C3-SynIIIa (gift from H.T. Kao) was digested, and the DNA fragment containing SynIIIa was cloned into the pCAGGs-IRES-tdTomato vector. The obtained pCAGGs-SynIIIa-IRES-tdTomato construct was used as a template in site-directed mutagenesis for the generation of the ShRNA-insensitive pCAGGs-rSynIIIa-IRES-tdTomato (rSynIII) construct. The mutagenesis protocols were performed with QuickChange lightning mutagenesis kit (Stratagene).

Silent mutations: (477C>T; 480C>T; 483T>C; 484C>T).

Silent mutations were generated in the targeting sequence of ShRNA#1 (470-490) 5'-AACCTGACTTCATTCTGGTTA-3' with the following primers:

FW 5’- GCGGTCCTTCAAACCTGATTTTATCTTGGTTAGACAGCATGCC -3’

RV 5’- GGCATGCTGTCTAACCAAGATAAAATCAGGTTTGAAGGACCGC -3’.

SynIII phosphomutants: S404A rSynIII and S404D rSynIII.

pCAGGs-rSynIIIa-IRES-tdTomato was used as a template for the generation of CDK5 phosphorylation site mutants. The non-phosphorylatable mutant (pCAGGs-SynIIIaS404A-IRES-tdTomato) was generated with the following primers:

FW 5’-CCTCGGTGCCCGCCCCCCTGAGACCTTG

RV 5’-CAAGGTCTCAGGGGGGCGGGCACCGAGG

This design allowed the replacement of the TCC codon encoding for Ser with the GCC codon encoding for Ala.

The pseudo-phosphorylated mutant (pCAGGs-SynIIIaS404D-IRES-tdTomato) was generated with the following primers:

FW 5’-CCTCGGTGCCCGACCCCCTGAGACCTTG

RV 5’-CAAGGTCTCAGGGGGTCGGGCACCGAGG

This design allowed the replacement of the TCC codon encoding for Ser with the GAC codon encoding for Asp.

To generate constructs for immunoprecipitation experiments, SynIII and its mutants were tagged at the amino terminal with 3XFLAG. pCAGGs-SynIII-IRES-tdTomato was digested, and the SynIII-containing fragment was cloned into the N-terminal p3XFLAG-CMV vector (Sigma). pEGFP-C1-SynIa (gift from H.T. Kao) was digested, and the DNA fragment containing SynIa was cloned into the pCAGGs-mCherry vector (gift from A. Contestabile). All of the constructs were

verified by sequencing. All of the enzymes were purchased by Promega Corporation, if not otherwise indicated.

COS7 Transfection

The day before transfection, 3.8 x 10^5 COS7 cells were plated on 6-cm plates. The medium was replaced with fresh medium 1 h before transfection. COS7 cells were co-transfected with 1.5 μg of SynIII cDNA and 3 μg of empty vector, ShRNAscr, ShRNA#1 or ShRNA#2 using Fugene 6 (Roche). For the *in vitro* phosphorylation assays, 6 x 10^5 COS7 cells were plated on 10-cm plates for 24 h and then and transfected with 2 μg of either FLAG-SynIIIa WT, FLAG-SynIIIa S404A cDNA or empty vector using Effectene (Qiagen). The cells were incubated at 37°C in a 5% CO_2 humidified atmosphere for 48 h and then processed for WB.

Neuronal Nucleofection and Immunofluorescence

Before plating, 4x10^6 neurons were transfected by electroporation with the Amaxa basal Nucleofector kit for primary neurons (Lonza) and 0.5 μg of plasmid DNA. The Amaxa Nucleofector device was used according to the manufacturer's protocol. For immunofluorescence, 3 DIV neurons were fixed with 4% PFA (Sigma) and 4% sucrose in phosphate-buffered saline (PBS), permeabilized/blocked with PBS containing 0.1% Triton X-100 and 3% BSA and then incubated with primary antibodies diluted in the same solution [anti-SynIII 1:800 (Synaptic System), anti-Smi 312, 1: 800 (Covance), anti-NP1, 1:100 (R&D

Systems), anti-p35, 1:50 (Abcam)]. Immunostaining was detected using Alexa 488, 546 or 647 fluorescent secondary antibodies (Invitrogen) diluted 1:500 in PBS containing 0.1% Triton X-100 and 3% BSA. The samples were mounted in Vectashield Mounting Medium (Vector Laboratories) and examined with confocal microscopy.

Western Blotting

The cells were lysed in lysis buffer (1% SDS, 1 mM EDTA, 10 mM HEPES, pH 7.4) supplemented with 1 mM PMSF, 10 mM NaF, complete mini EDTA-free protease inhibitor cocktail (Roche), phosphatase inhibitor cocktails (P0044, P5726; Sigma) and clarified by centrifugation (10 min at 20,000 x g). Rat cortices were lysed in lysis buffer (2% SDS, 2 mM EDTA, 10 mM HEPES, pH 7.4, 150 mM NaCl) supplemented with TissueLyserII (QIAGEN) by agitation with metallic beads. The lysates were boiled for 10 min, sonicated and clarified by centrifugation (15 min at 20,000 x g). The protein concentration of the samples was estimated using the BCA assay (Pierce). Equivalent amounts of protein were subjected to electrophoresis on 10% polyacrylamide NuPAGE precast gels (Invitrogen), according to the manufacturer's instructions. The gels were then transferred onto nitrocellulose membranes (Whatman), and the transfer quality was assessed by brief staining of the blot with 0.1% Ponceau stain. The blotted membranes were blocked for 1 h in 5% milk in Tris-buffered saline (10 mM Tris, 150 mM NaCl, pH 8.0) plus 0.1% Tween-20 and incubated overnight at 4°C with the following primary antibodies: anti-actin (1:5000, Sigma), anti-SynIII (RU486,

1:1000; Pieribone et al., 2002), anti-PSer404-SynIII (1:500, YenZym), anti-GADPH (1:1000, Sigma), anti-Syn domain E G304 (for SynIa and SynIIa, 1 :2000; Kao et al., 1998), anti-NP1 (1 :2000), and anti-CDK5 (1 :1000, Millipore). The anti-PSer404-SynIII antibody was a custom-made phospho-specific antibody generated by injecting a synthesized phosphorylated peptide into rabbits and double affinity-purification of the immune serum on dephospho- and phospho-peptide columns. The membranes were washed and incubated for 1 h at room temperature with peroxidase-conjugated anti-rabbit antibodies (1:5000; BioRad). The bands were revealed with SuperSignal West Pico chemiluminescent substrate (Pierce). Fluorograms were digitally scanned using an Epson V750 Pro Scanner (Seiko Epson Corporation), and band optical density (OD) was quantified using ImageJ software (RSB).

Co-Immunoprecipitation of SynIII-CDK5

Primary cultures of cortical neurons at 4 DIV were lysed in lysis buffer (50 mM Tris pH 7.4, 150 mM NaCl, 1 mM EDTA, 1% Triton X-100) supplemented with 1 mM PMSF and 10 mg/ml Pepstatin and clarified by centrifugation (10 min at 16,000 x g, 4°C). Equivalent amounts of cell extracts were incubated for 3 h at 4°C with either the RU486 anti-SynIII polyclonal antibody (10 μg/sample) or the anti-CDK5 monoclonal antibody (10 μg/sample; Millipore), which were pre-coupled with protein A and protein G Sepharose, respectively (25 μl of settled prewashed beads), or with Ctrl IgG. After extensive washing of the beads, the

sedimented immunocomplexes were subjected to SDS-PAGE and WB with anti-SynIII (1:1000) and anti-CDK5 (1:1000) antibodies.

Immunoprecipitation and *in Vitro* Protein Dephosphorylation/ Phosphorylation Assays

Following transient transfection, COS7 cells were washed three times in ice-cold HBSS (Gibco), scraped in lysis buffer (50 mM Tris pH 7.4, 150 mM NaCl, 1 mM EDTA, 1% Triton X-100; supplemented with 1 mM PMSF, 10 mg/ml pepstatin) and clarified by centrifugation (10 min at 16,000 x g, 4°C). The protein concentration was determined using the Bio-Rad protein assay (Biorad), and equivalent amounts of protein were incubated under rotation at 4°C with ANTI-FLAG M2 affinity gel (Sigma) that was pre-washed in lysis buffer. After 2 h, the bound proteins were washed three times with Tris-buffered saline (TBS), resuspended in phosphatase buffer (20 mM Tris pH 7.4, 100 mM NaCl, 5 mM $MgCl_2$, 1 mM $CaCl_2$, 0.5 mg/ml BSA, 1 mM DTT, 15 μg/ml calmodulin) and incubated with 2U calcineurin (Sigma) for 30 min at 30°C. The reaction was stopped by washing twice with ice-cold TBS. Phosphorylation was then initiated by adding 0.7 μg CDK5/p35 active enzyme (Millipore) in CDK5 reaction buffer (40 mM MOPS pH 7.0, 20 mM $MgCl_2$) in the presence of 50 μM [γ-^{32}P]ATP and 1.5 μCi/sample (specific activity 3000 mCi/mmol; Perkin Elmer) for 40 min at 30°C. After washing four times with TBS, bound radio-labeled proteins were resuspended in SDS-PAGE sample buffer, boiled for 2 min and resolved on 10%

acrylamide gels in SDS. The gels were stained with Coomassie blue and dried to analyze ^{32}P incorporation by autoradiography, followed by quantification with ImageQuant (GE Healthcare).

IUE

Briefly, E17 timed-pregnant Sprague-Dawley rats were anesthetized with isoflurane (induction, 3.5%; surgery, 2.5%), and the uterine horns were exposed by laparotomy. The day of confirmation of vaginal plug was defined as E0, and the day of birth was defined as P0. The DNA (0.15-1.5 µg/µl in water) together with the dye Fast Green (0.3 mg/ml; Sigma) was injected (5-6 µl) through the uterine wall into one of the lateral ventricles of each embryo using a 30G needle (Pic indolor). The embryo's head was carefully held between tweezer-type circular electrodes (10 mm diameter; Nepa Gene) that were wet with PBS while held across the uterine wall. For the electroporation protocol, 5 electrical pulses (amplitude, 50 V; duration, 50 ms; intervals, 150 ms) were delivered with a square-wave electroporation generator (CUY21EDIT; Nepa Gene). After electroporation, the uterine horns were returned into the abdominal cavity, and the embryos were allowed to continue their normal development. Given that the co-electroporation of two constructs *in vivo* leads to their concomitant expression in the vast majority of the transfected cells, the ShRNA constructs were always co-electroporated with the pCAGGs-IRES-tdTomato or EGFP vector (Fiumelli et al., 2005; Bony et al., 2013), which ensures both visualization of transfected cells

up to 1 month after birth (Cancedda et al., 2007) and balanced total plasmid mass in each electroporation.

Electrophysiology on brain slices

The rats were anesthetized with isoflurane and decapitated. Coronal slices (300 µm thickness) were cut using a Microm HM 650V microtome equipped with a Microm CU 65 cooling unit (Thermo Fisher Scientific) at 2°C in a solution containing (in mM): 87 NaCl, 25 $NaHCO_3$, 2.5 KCl, 0.5 $CaCl_2$, 7 $MgCl_2$, 25 glucose, and 75 sucrose and saturated with 95% O_2 and 5% CO_2. After cutting, the slices were left to recover for 30-45 min at 35°C and for 1 h at room temperature (RT) in the recording solution (see below). Whole-cell patch-clamp recordings were performed with a Multiclamp 700B/Digidata1440A system (Molecular Devices). tdTomato$^+$ PNs were selected for recording using an upright Olympus BX51WI microscope equipped with the appropriate filters (Olympus, Japan) and a Lambda LS lamp (Sutter). The extracellular solution used for recordings contained (in mM): 125 NaCl, 25 $NaHCO_3$, 2.5 KCl, 1.25 NaH_2PO_4, 2 $CaCl_2$, 1 $MgCl_2$ and 25 glucose (bubbled with 95% O_2 and 5% CO_2). For current-clamp experiments, the internal solution contained (in mM): 126 K-gluconate, 4 NaCl, 1 $MgSO_4$, 0.02 $CaCl_2$, 0.1 BAPTA, 15 glucose, 5 HEPES, 3 ATP, and 0.1 GTP (pH 7.3). Current-clamp recordings were performed at a holding potential of -70 mV, and action potential firing was induced by injecting current steps of 10

pA lasting 500 ms. All of the parameters were analyzed using pClamp (Molecular Devices) and the Prism (GraphPad Software, Inc.) software.

Slice Histology and Immunostaining

E21 brains were dissected and fixed for at least 24 hours in 4% PFA in PBS. P7-P14 brains were fixed by transcardial perfusion of 4% PFA in PBS. The brains were cryopreserved in 30% sucrose. The brains were frozen and sectioned coronally into 80 µm-thick sections with a microtome-refrigerator (Microm HM 450 Sliding Microtome equipped with Freezing Unit Microm KS34, Thermo Scientific). Free-floating slices were permeabilized and blocked with PBS containing 0.3% Triton X-100, 10% NGS and 0.2% BSA. The primary antibodies [mouse anti-NeuN (1:500; Chemicon) and rabbit anti-SynIII (RU316, 1:200; Kao et al., 1998), anti-βIII-tubulin (TUJ1,1 :400, Covance), anti-nestin (1 :100, Abcam), anti-γ-tubulin (1 :500, Sigma), anti-CUX1 (CDP, 1 :100, Santa Cruz), anti-CTIP2 (1 :100, Abcam) and anti-FOXP2 (1 :100, Abcam)] were incubated in PBS containing 0.3% Triton X-100, 5% NGS and 0.1% BSA. For CTIP2 staining, antigen retrieval was performed before blocking for 10 min at 95°C with citric acid buffer (10 mM, pH 6). For γ-tubulin staining, the slices were incubated at -20°C in ice-cold methanol for 10 min before blocking and permeabilization. Immunostaining was detected using Alexa 488 or Alexa 647 fluorescent secondary antibodies (Invitrogen) diluted 1:600 in PBS containing 0.3% Triton X-

100, 5% NGS and 0.1% BSA. The slices were counterstained with Hoechst (2,5 µg/µL; Sigma). The samples were mounted in Vectashield Mounting Medium (Vector Laboratories) and examined with confocal microscopy.

Confocal and Neurolucida Images Acquisition and Analysis

For analysis of migration at E21, images from sections that were counterstained with Hoechst were acquired using a confocal laser-scanning microscope (TCS SP5; Leica Microsystems) equipped with a 20 X immersion objective (NA 0.7). Confocal images of one slice for each experimental animal were acquired, and *Z*-series of confocal images were projected as two-dimensional (2-D) representations. To facilitate cell counting, the contrast of the images was adjusted to enhance the fluorescence of the cell bodies while attenuating the signal from neuronal processes. For representative pictures of P7/P14 neurons, 80-µm thick *z*-stacks were acquired with a 20 X immersion objective (NA 0.7), and *Z*-series of confocal images were projected as two-dimensional (2D) representations. For high-magnification images of cell morphology (ectopic cells and CP) and reconstructions of representative PNs, *z*-stacks covering the entire thickness of the cell of interest were acquired with a 40 X immersion objective (NA 1.25), and *Z*-series of confocal images were projected as 2D representations. To allow a better visualization of neuronal processes, the contrast of the images was adjusted to decrease the fluorescence of cell bodies. Reconstructions of representative PNs were drawn with Adobe Photoshop (Adobe System) using

these pictures as templates.

For analysis of the orientation of layer II/III PNs, 80-µm thick *Z*-stacks were acquired with a 40 X immersion objective (NA 1.25), and *Z*-series of confocal images were projected as 2D representations. The contrast of the images was adjusted to enhance the fluorescence of cell bodies and the apical dendrite while attenuating the signal from minor neuronal processes.

For analysis of ectopic cells at P7/P14, images from sections stained with an anti-Neu N antibody (for visualization of layer II/III) were acquired on an epifluorescence microscope equipped with a 10 X air objective (NA 0.3) and Neurolucida (MicroBrightField) software. The orientation of CP PNs was calculated using ImageJ by measuring the angle formed by the apical dendrite with the CP. UR PNs were defined as cells with apical dendrites making an angle between 45° and 135°with the pial surface. IN PNs were defined as cells with apical dendrites making an angle between 225° and 315° with the pial surface, and HOR PNs were the remaining cells. For all of the experiments, images of one slice per experimental animal were acquired.

For the correlation analysis of different fluorescence levels (Fig. S2E), images of cells were acquired with a 40 X immersion objective using a confocal laser-scanning microscope (TCS SP5; Leica Microsystems). One single focal plane was imaged at the level of the brightest tdTomato fluorescence for cells in the CP and ectopic PNs. The average fluorescence of the cell body was measured with LEICA SP5 software. The fluorescence of each cell was normalized to the average fluorescence for the cells in the same slice.

For dendrite morphology analysis, PNs were acquired using an epifluorescence microscope with a 40X air objective (NA 0.75) and traced with Neurolucida Neuron Tracing Software (MBF Bioscience). The traces were analyzed for total length and branches with NeuronJ (Plugin for ImageJ). Sholl analysis was performed manually using a mask made of concentric circles with increasing radii (10 μm distance each) and centered on the neuronal cell body.

For axonal orientation analysis, E18 brains were electroporated with ShRNA, LCK-GFP as an axonal marker and tdTomato, as previously described (Zuccaro et al., 2014). The brains were perfused and processed for microscopy at P7. The slices were analyzed using an epifluorescence microscope with a 40 X air objective. Cell orientation was verified through tdTomato fluorescence, axonal orientation was verified through GFP fluorescence and the axon was followed along its length as long as possible. Only cells with a clearly distinguishable axon were included in the analysis.

Mass spectrometry

Briefly, P1 rat pups were sacrificed. The cortices were dissected, put in lysis buffer (25 mM Tris pH 7.2, 137 mM NaCl, 10% glycerol, 1% Triton, 25 mM NaF, 1 mM Na3 VO4, 1 mM PMSF, 10 μg/μl leupeptin and 10 μg/μl pepstatin A) and dissociated first by pipetting up and down and then by passing the lysate through a 29 G needle. The homogenate was centrifuged at maximum speed in a table-top centrifuge for 15 min at 4°C. The supernatant was first pre-cleared for 1 h at

4°C and then incubated overnight at 4°C with anti-SynIII polyclonal antibodies (RU486; Kao et al., 1998). Lastly, the homogenate was incubated for 3 hours at 4°C with protein A Sepharose beads that were previously washed and equilibrated with lysis buffer. After incubation, the beads were washed with lysis buffer, resuspended in SDS-PAGE sample buffer 2X, boiled for 5 min and vortexed. The recovered sample was loaded on 10% polyacrylamide NuPAGE precast gels that were then stained with Blue Coomassie. The band corresponding to SynIII was cut out and processed for mass spectrometry analysis.

Tryptic peptides were resuspended in 2.5% FA and 2.5% MeCN and loaded using a Finnigan Micro AS Autosampler and a Finnigan Surveyor MS Pump Plus (Thermo Electron) onto a microcapillary column with a 100-µm inner diameter. The column was packed with 12 cm of reverse phase Magic C18 packing material (5 µm, 200 Å; Michrom Bioresources, Inc.). The flow rate over the column was 300-400 nl/minute. After a 14.5-min isocratic loading in 2.5% MeCN, 0.15% FA (Solvent A) peptides were eluted using a 5–35% gradient of Solvent B (99.85% MeCN, 0.15% FA) over 30 min and electrosprayed (1.8 kV) into a LTQ-Orbitrap Discovery mass spectrometer (Thermo Electron). The precursor scan (365-1600 *m/z*) was followed by ten collision-induced dissociation (CID) tandem mass spectra for the top 10 most abundant ions. The dynamic exclusion of the precursors chosen for MS/MS was enabled with a repeat count of three, a duration of 180 s, and an exclusion *m/z* width of $\pm$ 1.5. The AGC setting was 30,000, and the precursors were scanned with one microscan and a 10-ms

maximum injection time. The MS/MS scans had a 100-ms maximum injection time, a normalized collision energy of 35, an activation Q of 0.25, an activation time of 30 s and an isolation *m/z* width of ± 1. SEQUEST searches were performed using the *Rattus norvegicus* SynIII amino acid sequence as a database, requiring no enzyme specificity and allowing for the phosphorylation of serine, threonine and tyrosine (+79.9663 Da), the oxidation of methionine (+15.9949 Da), and the acrylamidation of cysteine (+71.0371 Da). All of the phosphopeptides were manually examined for phosphorylation site assignment, and phosphorylation localization assignments were also supported by Ascore software (Beausoleil et al., 2006).

Supplemental Results:

SynIII is expressed during cortical development *in vivo*

To investigate the role of SynIII in cortical development, we first addressed the expression pattern of its full-length isoform “a” (Porton et al., 1999) at various perinatal ages in rat cortices. SynIIIa was expressed at low levels at embryonic day 15 (E15), increased continuously to peak at postnatal day 7 (P7), and suddenly decreased to low levels at P16 and P35 (Figure S1A, B). In contrast, before P7, SynIa was present at lower levels than in the adult, while SynIIa was not expressed at detectable levels (Figure S1A, B). At E21, SynIII was present in

all cortical layers, with a high expression in the subventricular zone (SVZ) and cortical plate (CP, Figure S1C-F). SynIII$^+$ cells colocalized with nestin$^+$ neural progenitors in the VZ/SVZ (Figure S1C, D) and with tubulin β III$^+$ neurons in the CP (Figure S1E, F). At P7 and P14, SynIII expression was highest in the CP and decreased gradually to reach low levels in the VZ; SynIII$^+$ cells only colocalized with tubulin β III$^+$ PNs (Figure S1C-F).

SynIII downregulation does not affect neuronal identity, proliferation, or radial glia (RG) scaffold organization

Ectopic cells exhibited higher fluorescence intensity in comparison to CP cells, suggesting that the higher levels of ShRNA#1 expression (and thus, SynIII KD; Bony et al., 2013) correlated with larger defects (Figure S2E). Nonetheless, the ectopic PNs maintained their layer identity since they were CUX1$^+$ (layer II/III neuron marker; Figure S2C). Upon SynIII KD, although we found a strong defect in neuronal migration of the PNs, a process relying on radial glial (RG) fiber integrity, there was no significant impairment in the general architecture of the nestin$^+$ RG fiber scaffold (Figure S2D). Notably, we did not observe a significant difference in the number of daughter cells generated by the electroporated RG progenitors (Figure S2F), suggesting that KD did not affect cell proliferation.

SynIII regulates the morphological maturation but not basic electrophysiological proprieties of PNs

To investigate whether SynIII KD affects neuronal morphological maturation, we analyzed dendritic development in ShRNA-electroporated and control brains (Figure S4C). We found that neuronal orientation influenced dendritic morphology; IN cells in the CP or in ectopic positions displayed an increased mean length of dendritic branches in comparison to controls (Figure S4C). Moreover, Sholl analysis showed that misoriented PNs in the CP (HOR and IN) and UP ectopic cells displayed decreased complexity of the apical dendrite, while CP IN neurons showed decreased complexity of basal dendrites (Figure S4D).

We next addressed axonal development and found that regardless of their location, the majority of the ShRNA^{+} PNs had axons with an orientation that was opposite to that of the apical dendrite. Interestingly, the majority of the cells with no defined apical dendrite (i.e., HOR PNs) displayed an axon that still pointed to the ventricle, suggesting that external factors that repel/attract the axon play a key role in axonal orientation (Figure S4E).

We lastly used whole-cell patch-clamp recordings to assess whether the defects caused by SynIII KD in PNs impact their basic electrophysiological proprieties. SynIII ShRNA^{+} PNs displayed unaltered resting potential, passive membrane

properties (resistance, capacitance), action potential frequency and maximal firing rate compared to control cells (Figure S3F-L).

Supplemental discussion:

Tight spatial and temporal regulation of SynIII controls neuronal migration and orientation during development

A broad range of molecules, including transcription factors (e.g., MeCP2; Chao and Zoghbi, 2012) and proteins implicated in neuronal polarization (e.g., LKB1; Shelly et al., 2007; p75; Zuccaro et al., 2014) or cell migration (e.g., Reelin; Pujadas et al. 2010; Eriksson et al., 2001), have been described to be detrimental to normal cortical development both when knocked down/out and overexpressed. Commonly, the damaging effect of the KD/KO relies on the permanent loss of the pathway that the protein participates in. By contrast, the final outcome of an overexpression is not easily predicted, but this manipulation often results in the dysregulation of the protein's activity (e.g., MeCP2 over-dosage in Rett Syndrome, Chao and Zoghbi, 2012). The effect of SynIII overexpression described here could be due to the diffusion of the protein to parts of the cell where it is usually not expressed (e.g., dendrites), as our results show.

SynIII is part of the Sema3A pathway

The *in vitro* phosphorylation by CDK5 of the SynIII mutant, in which Ser^{404} was replaced by a non-phosphorylatable residue, was significantly lower than what we observed for the WT protein. The residual phosphorylation of S404A mutant may be due to other phosphorylation sites targeted by CDK5 or to the lack of regulatory mechanisms normally present in the cell (e.g., activator/inhibitor proteins, phosphatases), which leads other phosphorylatable residues to act as decoy sites.

The rescue experiments performed *in vivo* with phospho-mutants proved that Ser^{404} phosphorylation is functional and has a biological significance. Indeed, when expressed alone, the non-phosphorylatable mutant S404A rSynIII acted as a dominant negative on the endogenous protein, resulting in the appearance of ectopic cells. Interestingly, S404A rSynIII overexpression did not cause misorientation defects, suggesting that even a small fraction of endogenous phospho-SynIII is sufficient to control neuronal orientation. In accordance with the dominant negative effect, S404A rSynIII, unlike WT rSynIII, was unable to rescue the defects caused by SynIII KD. Consistent with this, we observed that the pseudo-phosphorylated mutant S404D rSynIII partially rescue the delay in radial migration caused by SynIII KD. The lack of a full rescue may be due to the inability of the S404D rSynIII mutant to cycle between phosphorylated and

dephosphorylated states. Nonetheless, these results suggest that the phosphorylation of SynIII by CDK5 is essential for SynIII's role in radial migration and that the phenotype we observed in SynIII-null PNs is at least partially due to a missing step in CDK5 signaling.

By means of a custom-made phospho-specific antibody against the phosphorylated Ser^{404} residue of SynIII, we showed that phosphorylation increased upon Sema3A stimulation, proving that SynIII is a downstream effector of Sema3A/CDK5 signaling. Additionally, the expression of the Sema3A receptor NP1 during cortical development strongly resembled the expression pattern of SynIII at the same ages, and the two proteins colocalized in developing neurons in culture. Further confirming the data above, our *in vivo* data showed a significant rescue of the defect in radial migration caused by NP1 KD by *in utero* co-transfection of the pseudo-phosphorylated mutant S404D rSynIII. As this mutant mimics SynIII phosphorylation by CDK5 upon Sema3A activation, its presence may partially compensate for the loss of Sema3A signaling caused by NP1 KD. Thus, our data demonstrate that SynIII is part of the Sema3A III pathway (Figure 7I).

Hypothetical mechanisms of action of SynIII

Neuronal migration is strongly affected in neurons with defective axon/dendrite polarization (Shelly et al., 2007; Shelly et al., 2011; Zuccaro et al., 2014). Although we found defects in dendrite morphology and axonal orientation in SynIII-KD PNs, we did not directly analyze a possible defect in neuronal polarization due to SynIII KD. Nevertheless, *in vitro* data from the literature suggest that polarization defects may occur (Ferreira et al., 2000; Feng et al., 2002). As SynIII carries a phosphorylation site for PKA, its functions with respect to polarization may also be regulated by Sema3A through negative regulation of cAMP production and consequent PKA activity (Shelly et al., 2011). Lastly, our partially penetrant phenotype could be due to SynIII being only one component of a Sema3A-directed program, as many different molecules act downstream of Sema3A (e.g., the CRMP family, Schmidt and Strittmatter, 2007) to coordinate multiple aspects of neuronal development.

Beausoleil, S.A., Villen, J., Gerber, S.A., Rush, J., and Gygi, S.P. (2006). A probability-based approach for high-throughput protein phosphorylation analysis and site localization. Nature biotechnology *24*, 1285-1292.
Cancedda, L., Fiumelli, H., Chen, K., and Poo, M.M. (2007). Excitatory GABA action is essential for morphological maturation of cortical neurons in vivo. J Neurosci *27*, 5224-5235.
Chao, H.T., and Zoghbi, H.Y. MeCP2: only 100% will do. Nat Neurosci *15*, 176-177.
Elbashir, S.M., Harborth, J., Lendeckel, W., Yalcin, A., Weber, K., and Tuschl, T. (2001). Duplexes of 21-nucleotide RNAs mediate RNA interference in cultured mammalian cells. Nature *411*, 494-498.
Eriksson, S.H., Thom, M., Heffernan, J., Lin, W.R., Harding, B.N., Squier, M.V., and Sisodiya, S.M. (2001). Persistent reelin-expressing Cajal-Retzius cells in polymicrogyria. Brain : a journal of neurology *124*, 1350-1361.

Fiumelli, H., Cancedda, L., and Poo, M.M. (2005). Modulation of GABAergic transmission by activity via postsynaptic Ca2+-dependent regulation of KCC2 function. Neuron *48*, 773-786.
Pieribone, V.A., Porton, B., Rendon, B., Feng, J., Greengard, P., and Kao, H.T. (2002). Expression of synapsin III in nerve terminals and neurogenic regions of the adult brain. J Comp Neurol *454*, 105-114.
Pujadas, L., Gruart, A., Bosch, C., Delgado, L., Teixeira, C.M., Rossi, D., de Lecea, L., Martinez, A., Delgado-Garcia, J.M., and Soriano, E. Reelin regulates postnatal neurogenesis and enhances spine hypertrophy and long-term potentiation. J Neurosci *30*, 4636-4649.
Schmidt, E.F., and Strittmatter, S.M. (2007). The CRMP family of proteins and their role in Sema3A signaling. Advances in experimental medicine and biology *600*, 1-11.
Shelly, M., Cancedda, L., Heilshorn, S., Sumbre, G., and Poo, M.M. (2007). LKB1/STRAD promotes axon initiation during neuronal polarization. Cell *129*, 565-577.